New genetic tools for mushroom body output neurons in *Drosophila*

Gerald M. Rubin[1,✉] **and Yoshinori Aso**[1,✉]

[1]Janelia Research Campus, Howard Hughes Medical Institute, Ashburn, VA 20147, USA

Abstract

How memories of past events influence behavior is a key question in neuroscience. The major associative learning center in *Drosophila*, the Mushroom Body (MB), communicates to the rest of the brain through Mushroom Body Output Neurons (MBONs). While 21 MBON cell types have their dendrites confined to small compartments of the MB lobes, analysis of EM connectomes revealed the presence of an additional 14 MBON cell types that are atypical in having dendritic input both within the MB lobes and in adjacent brain regions. Genetic reagents for manipulating atypical MBONs and experimental data on their functions has been lacking. In this report we describe new cell-type-specific GAL4 drivers for many MBONs, including the majority of atypical MBONs. Using these genetic reagents, we conducted optogenetic activation screening to examine their ability to drive behaviors and learning. These reagents provide important new tools for the study of complex behaviors in *Drosophila*.

Mushroom Body | Central Complex | Learning and Memory | Dopamine | *Drosophila melanogaster*

Correspondence:
rubing@janelia.hhmi.org,
asoy@janelia.hhmi.org

Introduction

The Mushroom Body (MB) is the major site of associative learning in insects (reviewed in (1–3)). In the MB of each Drosophila brain hemisphere, multiple modalities of sensory stimuli are represented by the sparse activity of 2000 Kenyon cells (KCs) whose parallel axonal fibers form the MB lobes. The lobes are further divided into compartments by the innervation patterns of dopaminergic neuron (DAN) axons and mushroom body output neuron (MBON) dendrites. MBONs provide the convergence element of the MB's three layer divergent-convergent circuit architecture and the outputs of the MBONs drive learned behaviors.

Whereas the dendrites of typical MBONs are strictly confined to the MB lobes, analysis of the Drosophila connectome (3, 4) revealed a new class of "atypical" MBONs, consisting of 14 cell types, that have part of their dendritic arbors outside the MB lobes, allowing them to integrate input from KCs with other information (3). Some atypical MBONs receive dendritic input from other MBONs. Several provide output onto dopaminergic neurons (DANs) that innervate the MB to participate in recurrent networks. At least five make strong, direct synaptic contact onto descending neurons that drive motor action. Three provide strong direct connections to tangential neurons of the fan-shaped body of the central complex. However, analysis of the behaviors mediated by atypical MBONs has been limited by the lack of genetic drivers needed to manipulate their activity.

Here we report the generation and characterization of cell-type-specific split-GAL4 driver lines for the majority of the atypical MBONs. We also provide driver lines for two typical MBON types for which cell-type-specific split-GAL4 drivers were not previously available, and improved drivers for several other MBONs. We demonstrate the use of these new split-GAL4 lines in two behavioral assays. Using a four-armed olfactory arena equipped with optogenetic LED panels (5, 6), we assessed the ability of the labeled neurons to act as the unconditioned stimulus in an olfactory learning assay, an indication of their regulation of the acitivity of DANs. We also measured the effects of their optogenetic activation on kinematic parameters relevant for olfactory navigation. These reagents provide important new tools for the study of complex behaviors in *Drosophila*.

Results and Discussion

Generation and characterization of split-GAL4 lines for MBONs. We generated split-GAL4 genetic driver lines corresponding to MBON cell type using well-established methods (7–10). The morphologies of the MBONs, produced by electron microscopic reconstruction, were used to search databases of light microscopic images to identify enhancers whose expression patterns might yield clean driver lines for that MBON when intersected (11, 12). We took advantage of an expanded set of starting reagents that were not available when we (13) generated the original set of split-GAL4 drivers for the MB cell types; in addition to the 7,000 GAL4 expression patterns described in (14), we had access to an additional 9,000 GAL4 expression patterns (10). A total of approximately 600 intersections were experimentally tested to generate the split-GAL4 lines reported here.

Figure 1 shows examples of expression patterns of some of the highest quality split-GAL4 lines. For many cell types we were able to identify multiple different split-GAL4 lines. The brain and ventral nerve cord expression patterns of all split-GAL4 lines are shown in Figure supplement 1 for atypical MBONs and Figure supplement 2 for typical MBONs. The original confocal stacks from which these Figures were generated, as well as additional image data, are available for download at https://splitgal4.janelia.org. Videos 1 and 2 provide examples of comparisons between light microscopic images from these lines and neuronal skeletons from the hemibrain dataset (4) that were used to confirm the assignment of

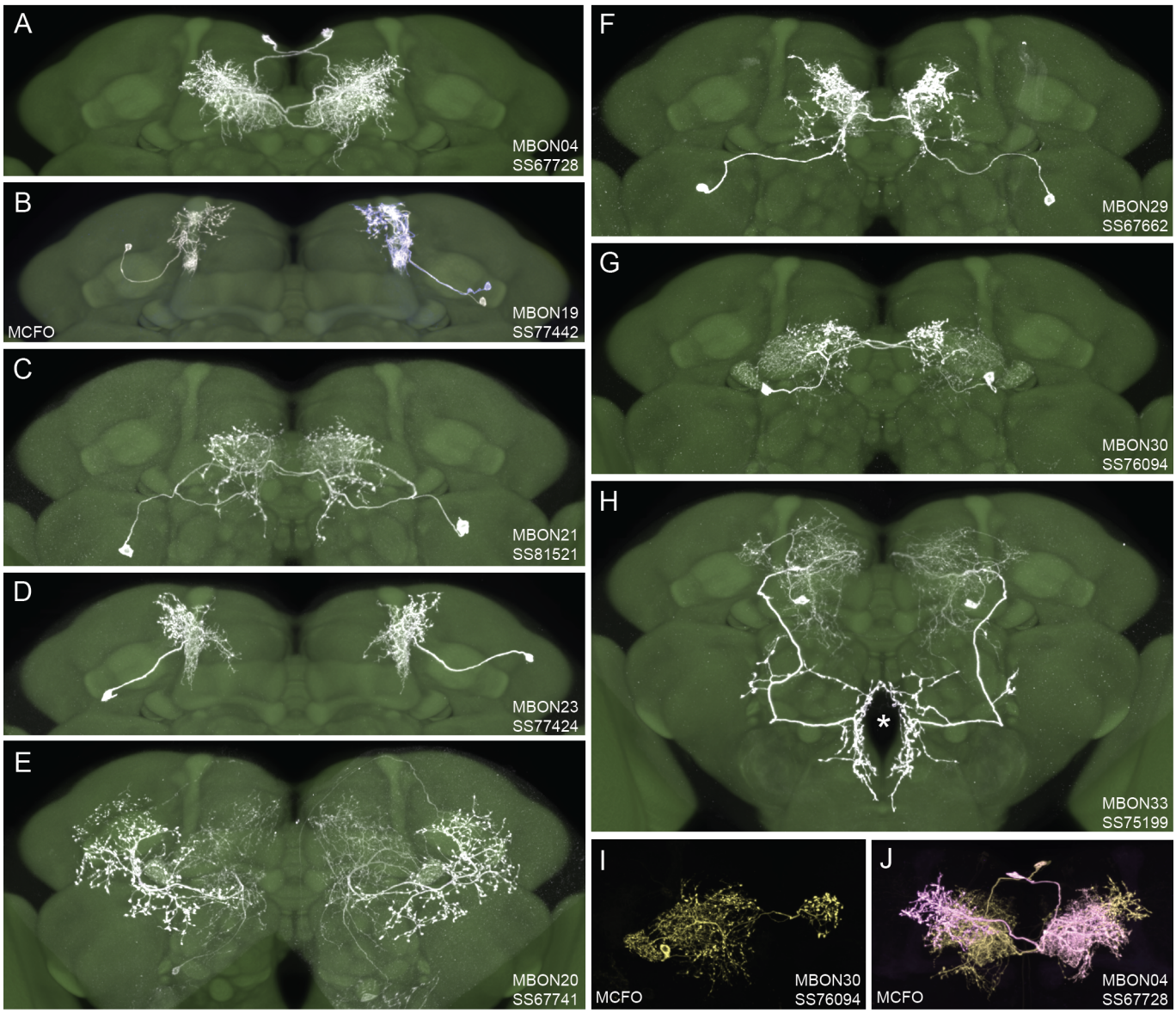

Fig. 1. Selected images of new split-GAL4 lines. Panels A and C-H show expression (maximum intensity projections) of the indicated split-GAL4 line in the relevant portion of the brain. In panels A-H, the consensus JFRC2018 unisex brain template is also shown (green). The asterisk in panel H indicates the position of the esophagus. Images showing the full brain, optic lobe and ventral nerve cord of these lines can be found in Figure supplement 1 (for E-H) and Figure supplement 2 (for A-D). Panels B, I and J show images derived from stochastic labeling that reveal the morphology of individual cells. The original confocal stacks from which these images were derived are available for download at https://splitgal4.janelia.org/.

cell type identity. Figure supplement 3 summarizes what we consider to be the best available split-GAL4 lines for each of the MBON types identified by connectomics, based on a combination of the lines presented here and in previous studies.

For typical MBONs, we provide split-GAL4 lines for two cell types for which drivers were not described in (13), MBON21 and MBON23. We also provide improved lines for MBON04 and MBON19; previous drivers for MBON04 also had expression in other MBON cell types and our new line for MBON19 has less off-target expression (see (13) for previous lines).

For atypical MBONs we were able to generate multiple, independent driver lines for MBON20, MBON29, MBON30 and MBON33 that provide strong and specific expression. Several lines for MBON31 were generated, but they also stochastically express in MBON32. Lines for MBON26 and MBON35 have some off-target expression that might compromise their use in behavioral assays, but they should permit cell-type-specific imaging studies. We failed to generate lines for MBON24, MBON25, MBON27, MBON32 and MBON34; we identified 2 candidate lines for MBON28 (see Figure supplement 3).

Activation phenotypes of MBON lines. MBONs are the first layer of neurons that transform memories stored inside the MB into actions. MBONs can also provide input to the dendrites of the DANs that innervate the MB lobes, forming a recurrent network. To investigate these two aspects of MBON function, we used a four-armed olfactory arena

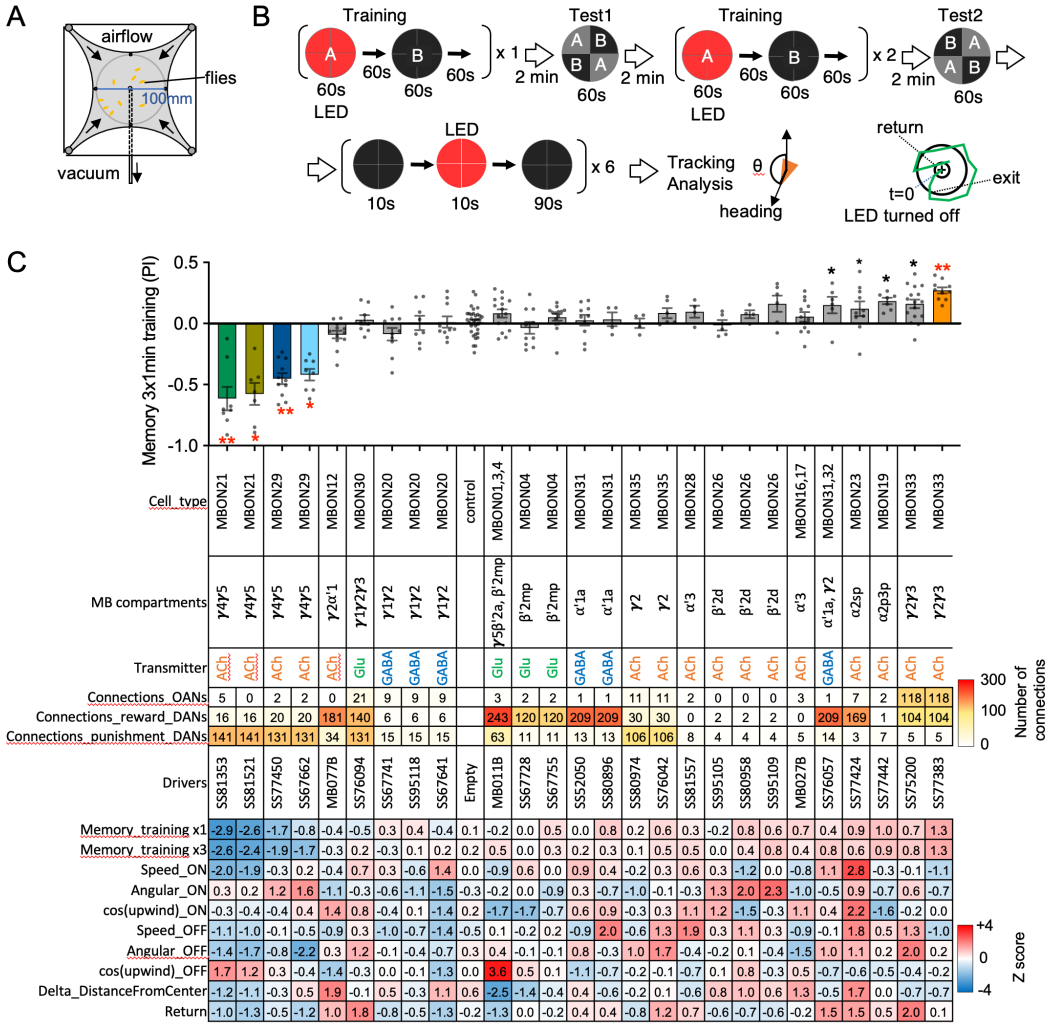

Fig. 2. Behavioral consequences of optogenetic activation. (A) Diagram of the four-armed olfactory arena. Approximately 20 starved female flies were confined in 10 cm diameter and 3 mm high circular area with a hole at the center for air suction. Odor was introduced through four channels at the corners. (B) The protocol for behavioral experiments. Flies were trained by pairing 60 s of odor A with 30 1-second pulses of 627 nm LED light, each separated by 1 s without illumination. A different odor, odor B, was presented without red LED illumination, and then the preference between two odors was tested. In the reciprocal experiments, odor B was paired with red light and odor A was unpaired. The same training was repeated twice more and then a second odor preference test was performed. Finally, six cycles of 10-second 627 nm illumination were applied, spaced by 100 s intervals without odor. Airflow was maintained at 400 mL/min throughout the experiment. (C) Top: The memory scores at the second odor preference test, measured as a preference index defined as the [(number of flies in the paired odor quadrants)-(number of flies in the unpaired odor quadrants)]/total number of flies during the last 30 s of the 60 s test period. The red asterisks * and ** indicate $p<0.05$ or $p<0.01$, respectively: Dunn's multiple comparison tests compared to empty-split-GAL4 control, following Kruskal-Wallis test. The black * indicates $p<0.05$ without correction for multiple comparison. N=34 for the empty-split-GAL4 line and N=4-16 for other lines. All the lines were initially tested in 4 reciprocal experiments; lines with mean preference index above 0.1 or below -0.1 were subjected to additional tests. Cell types, the MB compartments in which their dendrites lie, their neurotransmitters, the number of synaptic connections they make with dopaminergic (DANs) and octopaminergic (OANs) neurons, and the split-GAL4 driver lines used for the behavioral assays are designated. A summary of connections from all MBON subtypes to DANs thought to signal reward or punishment and to OANs is shown in Figure supplement 4A. Bottom: Z-scores [(values-mean)/standard deviation] for each parameter: Speed, walking speed; Angular, absolute of angular change relative to the previous frame at 30 FPS; cos(upwind), cosine of the fly's orientation toward the upwind direction (that is, facing away from the center of the arena). ON periods correspond to the first 2 s of the 10 s LED ON periods, whereas OFF periods are the 2 s immediately after the LEDs were turned off. ΔDistanceFromCenter is change in fly's mean distance from the center of the arena relative to its position at the onset of LED illumination. Return is a measure of the probability that a fly returns to the position that it occupied at the end of the LED stimulus. Flies are judged to have returned if they move 10 mm or more from their original position and then return to within 3 mm of the original position within 15 s.

equipped with LED panels for optogenetics (Figure 2A). A group of 20 starved flies that express CsChrimson in a particular MBON cell type was subjected to a series of optogenetic olfactory conditioning and memory tests, and then to six trials of activation in the absence of odors but with airflow (Figure 2B). Using the same setup and similar protocols, we have previously characterized the dynamics of memories formed by optogenetically activating DAN cell types innervating different MB compartments (6) and analyzed circuits downstream of the MBONs that promote upwind locomotion (15). Figure 2C displays the results of these behavioral experiments sorted by the mean memory score of each cell type in the final memory test. When possible, we ran multiple independent split-GAL4 lines for the same MBON cell type. The concurrence of phenotypes in these cases provides further evidence that the observed effects are due to the activation of that cell type rather than off-target expression or genetic background effects.

Training flies by paring odor presentation with activation of MBON21, using either of the two lines tested (SS81353 and

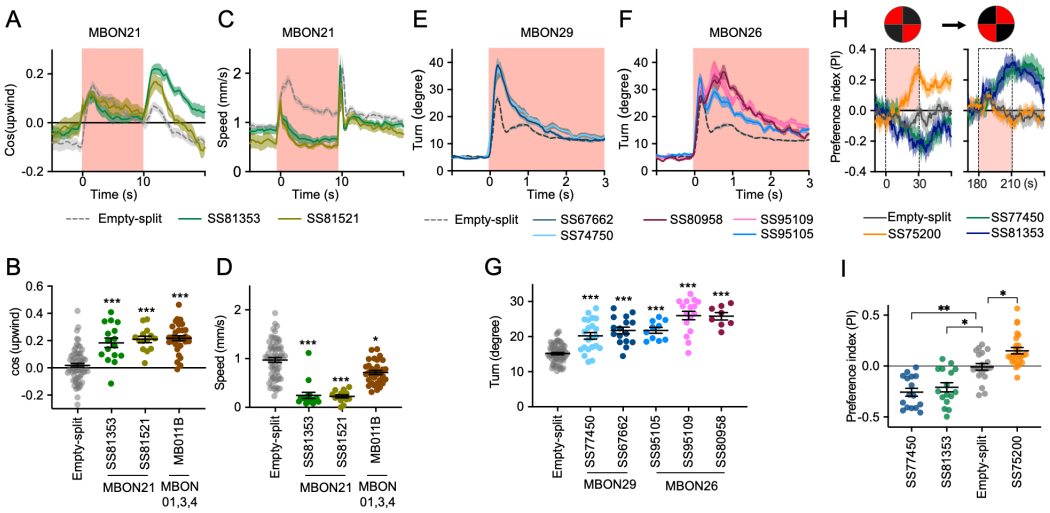

Fig. 3. Additional behavioral consequences of optogentic activation. (A) Time course of mean cos (upwind angle) for flies that express CsChrimson using the designated MBON21 drivers. The trace of empty-split-GAL4 is also shown. Red shading indicates the periods of 627 nm LED illumination. The trajectories from six trials were pooled to calculate a mean for each group of flies. Lines and shadings represent means and SEMs. (B) Mean cos(upwind angle) during the 2 s immediately after the LED was turned off. (C-D) Time course and mean walking speed during the 10 s LED On period. (E-F) The mean cumulative turning angles in 5 movie frames (total elapsed time of 150 ms) for flies expressing CsChrimson in MBON29 and MBON26. (G) The cumulative turning angle during the first 2 s of the LED On period. (A-G) show data from the experiments described in Figure 2. (H) Preference for quadrants with red light. Flies expressing CsChrimson in MBON21, MBON29 or MBON33 were tested with 30 s continuous light (627nm LED) in two quadrants. The test was performed a second time with illumination in opposite quandrants after an 150 s recovery period. (I) Mean preference index to the quadrants with red light during the last 5 s of the two 30 s test periods. Dunn's multiple comparison tests compared to empty-split-GAL4 control, following Kruskal-Wallis test. *, ** and *** indicate p<0.05, p<0.01 or p<0.001, respectively: N=66 for Empty-split-GAL4 and 8-22 for other lines in (A-G). N=16-26 in (H-I).

SS81521), resulted in robust aversive memory (Figure 2C) as previously observed with another driver for this cell type that displayed weaker expression (see SS46348 in Figure supplement 2; (16)). Both driver lines for the atypical MBON29 similarly induced aversive memory. These MBONs are both cholinergic, have dendrites in the $\gamma4$ and $\gamma5$ compartments, and synapse onto the dendrites of DANs that respond to punitive stimuli such as PAM-$\gamma3$ and PPL1-$\gamma1$pedc (Figure 2C, Figure supplement 4; (3, 16)). In contrast, training flies with activation of MBON33 induced appetitive memory. MBON33 is also cholinergic but preferencially connects with octopaminergic neurons and reward-representing DANs. We noticed that confocal microscopy images of MBON33 visualized by split-GAL4 driven expression contains additional branches around the esophagus (Figure 1H), an area which was outside of EM hembrain volume. Since octopaminergic neurons arborize in this area (17), the connection between MBON33 and octopaminergic neurons might be more extensive than the previously described using the hemibrain data (3).

To explore kinematic parameters controlled by MBONs, we tracked the trajectories of individual flies during and after a 10-second optogenetic stimulus (Figure 2C). In these assays we observed some variability between lines for the same cell type, presumably due to difference in expression level or off-targeted expression. Nevertheless, the two lines for MBON21 showed similar patterns of kinematic variables: a low walking speed in the presence of the red activation light, a stimulus that caused elevated locomotion in genetic control flies, and then orientation toward upwind when the optogenetic stimulus concluded (Figures 2C and 3A-D). Similar phenotypes were observed with a driver for a combination of three glutamatergic MBONs: MBON01, MBON03 and MBON04 (MB011B; Figure 2C). Despite their common anatomical features and memory phenotypes, MBON21 and MBON29 modulated distinct motor parameters. Neither of the two lines for MBON29 changed walking speed or orientation toward upwind when activated, but they both increased angular motion at the onset of activation, similar to three lines for MBON26 (Figure 3E-G).

Finally, we asked if the MBON21, MBON29 and MBON33 lines that were able to serve as the unconditioned stimulus in memory formation also drove avoidance or attraction of corresponding valence. Previous studies and the results shown in Figures 2C indicated that these are not always shared phenotypes; for example, the set of glutamatergic MBONs in MB011B whose dendrites lie in the $\gamma5$ and $\beta'2$ compartments, can drive downwind locomotion and avoidance behaviors (26–28) but do not induce aversive memory. We tested if flies expressing CsChrimson in each of these three MBON cell types prefer quadrants of the arena with red activating light during the first and second 30 s test periods (Figure 3H,I). When CsChrimson is expressed in MBON21 or MBON29, flies avoided illuminated quadrants of the arena. Conversely, CsChrismon activation in a line for MBON33 promoted attraction to illuminated quadrants, although this effect was observed only at the first test period. Thus, in the case of these three MBON cell types, memory formation and avoidance/attraction behaviors are correlated.

Concluding Remarks

We generated and anatomically characterized an improved set of genetic driver lines for MBONs and provide the first driver lines for atypical MBONs. We expect these lines to be useful in a wide range of studies of fly behavior. We

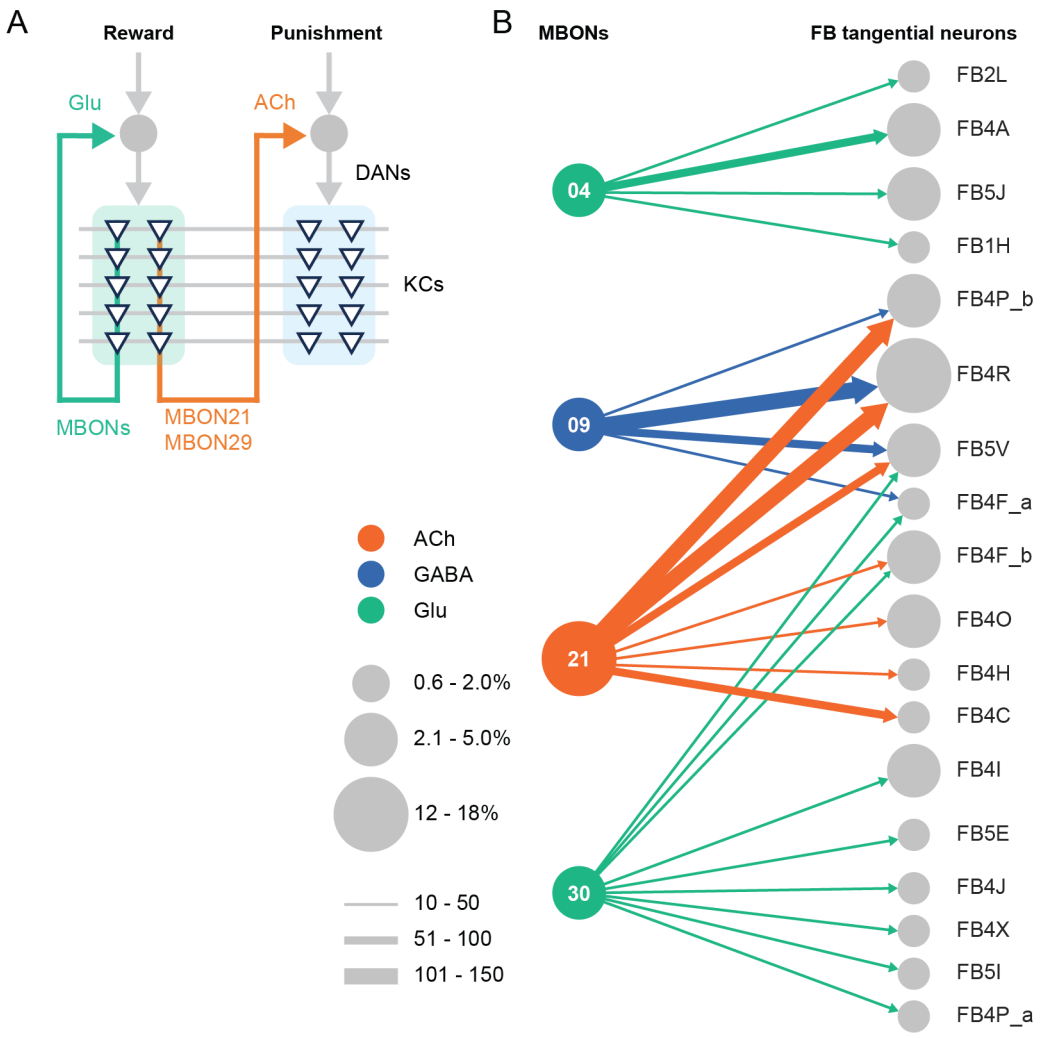

Fig. 4. Diagrammatic summary of key outputs from selected MBONs. (A) MBON21 and MBON29 arborize dendrites in the γ4 and γ5 compartments that are innervated by reward representing DANs. MBON21 and MBON29 are cholinergic and preferentially connect with DANs that innervate other compartments to represent punishment, whereas other glutamtergic MBONs from these same compartments preferentially form connections with reward representing DANs going back to the same compartments. In the fly brain, acetylcholine (ACh) is largely excitatory via nicotinic ACh receptors, although the type A muscarinic ACh receptor can mediate an inhibitory effect (18, 19). Glutamate (Glu) can be inhibitory or excitatory depending on the receptors in the postsynaptic cells. Glutamate is known to be inhibitory via the glutamate-gated chrolide channel (GluClα) in the olfactory system (20). All of the ten types of DANs examined with RNA-seq express GluClα and Nmdar2 at high levels whereas expression of Nmdar1 and other glutamate receptors were limited and cell type specific (21). Results in some studies support an excitatory effect of at least a subset of glutamatergic MBONs on DANs (16, 22–24), while electrophysiological recordings indentified inhibitory connection between a glutamatergic MBON and downstream interneurons (15). (B) Diagram showing direct connections between the MB and CX mediated by MBON21, MBON30, MBON09 and MBON04; these MBONs rank first, second, fifth and seventh, respectively, based on the number of direct synaptic connections to the CX; numbers reflect connections between right hemisphere MBONs and right hemisphere FB tangential cells. For circles representing MBONs, the circle diameter represents the fraction of that MBONs direct output that goes to the CX. For the downsteam neurons in the CX, circle diameter represents the fraction of that cell types direct input that comes from MBONs. Arrow width reflects synapse number. See Figure 19 of (3) and Figure 46 of (25) for additional information on the complete set of MB to CX connections.

demonstrate the suitability of these lines for behavioral analyses by showing that multiple independent lines for the same cell type gave consistent results when assayed for their ability to serve as the unconditioned stimulus in memory formation and to produce appetitive or aversive movements. MBON21, MBON29 and MBON33, characterized in this study, have dinstint features compared to well-studied MBONs that arborize in the same compartments. MBON21 and MBON29 form cholingergic connections to the dendrites of DANs known to respond to punishment, whereas other MBONs from the same compartments form glutamatergic connections with reward-representing DANs (Figure 4A).

While most sensory input to the MB is olfactory, the connectome revealed that two specific classes of Kenyon cells receive predominantly visual input. MBON19 provides the major output from one of these classes, KCα/βp, and about half of MBON19's sensory input is estimated to be visual. MBON33 provides a major output from the other class of visual KCs, KCγd, with more than half of the sensory input to its dendrites in the MB estimated to be visual. The cell-type-specific driver lines we provide for MBON19 and MBON33 should facilitate studies of the behavioral roles of the two streams of visual information that pass through the MB.

The MB and the central complex (CX) are thought to play key roles in the most cognitive processes that the fly can perform including learning, memory, and spatial navigation. Two of the MBONs for which we generated cell-type-specific driver

lines, MBON21 and MBON30, provide the strongest direct inputs to the CX from the MB (Figure 4B), while MBON30 receives over three percent of its input (450 synapses) from the CX cell type FR1. The genetic reagents we report here should advance studies of reinforcement signals in parallel memory systems, the role of visual inputs to the MB, and information flow from the MB to the CX.

Methods and Materials

Flies. Split-GAL4 lines were created as previously described (7). Flies were reared on standard cornmeal molasses food at 21-22°C and 50% humidity. For optogenetic activation experiments, flies were reared in the dark on standard food supplemented with retinal (Sigma-Aldrich, St. Louis, MO) unless otherwise specified, 0.2 mM all trans-retinal prior to eclosion and 0.4 mM all trans-retinal post eclosion. Female flies were sorted on cold plates and kept in retinal food vials for at least 1 day prior to be transferred to agar vials for 48-72 hours of starvation. Flies were 4-10 day old at the time of behavioral experiments.

Immunohistochemistry and imaging. Dissection and immunohistochemistry of fly brains were carried out as previously described (13). Each split-GAL4 line was crossed to the same Chrimson effector used for behavioral analysis. Full step-by-step protocols can be found at https://www.janelia.org/project-team/flylight/protocols. For single-cell labelling of neurons from selected split-GAL4 lines, we used the MultiColor FlpOut (MCFO) technique (29). Video 1 and Video 2 were produced using VVD Viewer (https://github.com/JaneliaSciComp/VVDViewer) to generate a video comparing light and EM data (hemibrain v1.2) for each cell type. Individual videos were then concatenated, and text added using Adobe Premiere Pro.

Optogenetics and olfactory learning assays. Groups of approximately 20 female flies were trained and tested at 25°C at 50% relative humidity in a fully automated olfactory arena for optogenetics experiments as previously described (5, 6, 30). The 627 nm peak LED light was used at 22.7 $\mu W/mm^2$. The odors were diluted in paraffin oil (Sigma–Aldrich): Pentyl Acetate (PA; 1:10000) and Etyl Lactate (EL; 1:10000). Videography was performed at 30 frames per second with a 850 nm LED backlight with a 820 nm longpass filter and analyzed using the Flytracker (31) and Fiji (32).

Statistics. Statistical comparisons were performed using the Kruskal Wallis test followed by Dunn's post-test for multiple comparison (Prism; Graphpad Inc, La Jolla, CA 92037). Appropriate sample size for olfactory learning experiment was estimated based on the standard deviation of performance index in a previous study using the same assay (6).

Connectomics. Information on connection strengths are taken from neuprint.janelia.org (hemibrain v1.2.1).

ACKNOWLEDGEMENTS
We thank the Janelia Fly Facility for help with fly husbandry and the FlyLight Project Team for dissection, histological preparation, and imaging of nervous systems. We thank Janelia Project Technical Resources for carrying out EASI-FISH assays. Marisa Dreher (Dreher Design Studios, Inc.) assembled the videos and helped with figure design. Claire Managan segmented the neuron morphologies shown in the videos. Masayoshi Ito helped identify lines to use in intersections. We thank Vivek Jayaraman, Daisuke Hattori, Yichun Shuai and Toshihide Hige for comments on earlier drafts of the manuscript.

Bibliography

1. Martin Heisenberg. Mushroom body memoir: from maps to models. *Nature Reviews Neuroscience*, 4(4):266–275, April 2003. ISSN 1471-0048. doi: 10.1038/nrn1074.
2. Mehrab N. Modi, Yichun Shuai, and Glenn C. Turner. The Drosophila Mushroom Body: From Architecture to Algorithm in a Learning Circuit. *Annual Review of Neuroscience*, 43: 465–484, July 2020. ISSN 1545-4126. doi: 10.1146/annurev-neuro-080317-0621333.
3. Feng Li, Jack W Lindsey, Elizabeth C Marin, Nils Otto, Marisa Dreher, Georgia Dempsey, Ildiko Stark, Alexander S Bates, Markus William Pleijzier, Philipp Schlegel, Aljoscha Nern, Shin-ya Takemura, Nils Eckstein, Tansy Yang, Audrey Francis, Amalia Braun, Ruchi Parekh, Marta Costa, Louis K Scheffer, Yoshinori Aso, Gregory SXE Jefferis, Larry F Abbott, Ashok Litwin-Kumar, Scott Waddell, and Gerald M Rubin. The connectome of the adult Drosophila mushroom body provides insights into function. *eLife*, 9:e62576, December 2020. ISSN 2050-084X. doi: 10.7554/eLife.62576.
4. Louis K Scheffer, C Shan Xu, Michal Januszewski, Zhiyuan Lu, Shin-ya Takemura, Kenneth J Hayworth, Gary B Huang, Kazunori Shinomiya, Jeremy Maitlin-Shepard, Stuart Berg, Jody Clements, Philip M Hubbard, William T Katz, Lowell Umayam, Ting Zhao, David Ackerman, Tim Blakely, John Bogovic, Tom Dolafi, Dagmar Kainmueller, Takashi Kawase, Khaled A Khairy, Laramie Leavitt, Peter H Li, Larry Lindsey, Nicole Neubarth, Donald J Olbris, Hideo Otsuna, Eric T Trautman, Masayoshi Ito, Alexander S Bates, Jens Goldammer, Tanya Wolff, Robert Svirskas, Philipp Schlegel, Erika Neace, Christopher J Knecht, Chelsea X Alvarado, Dennis A Bailey, Samantha Ballinger, Jolanta A Borycz, Brandon S Canino, Natasha Cheatham, Michael Cook, Marisa Dreher, Octave Duclos, Bryon Eubanks, Kelli Fairbanks, Samantha Finley, Nora Forknall, Audrey Francis, Gary Patrick Hopkins, Emily M Joyce, SungJin Kim, Nicole A Kirk, Julie Kovalyak, Shirley A Lauchie, Alanna Lohff, Charli Maldonado, Emily A Manley, Sari McLin, Caroline Mooney, Miatta Ndama, Omotara Ogundeyi, Nneoma Okeoma, Christopher Ordish, Nicholas Padilla, Christopher M Patrick, Tyler Paterson, Elliott E Phillips, Emily M Phillips, Neha Rampally, Caitlin Ribeiro, Madelaine K Robertson, Jon Thomson Rymer, Sean M Ryan, Megan Sammons, Anne K Scott, Ashley L Scott, Aya Shinomiya, Claire Smith, Kelsey Smith, Natalie L Smith, Margaret A Sobeski, Alia Suleiman, Jackie Swift, Satoko Takemura, Iris Talebi, Dorota Tarnogorska, Emily Tenshaw, Temour Tokhi, John J Walsh, Tansy Yang, Jane Anne Horne, Feng Li, Ruchi Parekh, Patricia K Rivlin, Vivek Jayaraman, Marta Costa, Gregory SXE Jefferis, Kei Ito, Stephan Saalfeld, Reed George, Ian A Meinertzhagen, Gerald M Rubin, Harald F Hess, Viren Jain, and Stephen M Plaza. A connectome and analysis of the adult Drosophila central brain. *eLife*, 9:e57443, September 2020. ISSN 2050-084X. doi: 10.7554/eLife.57443.
5. Jan Pettersson. An Aphid Sex Attractant. *Insect Systematics & Evolution*, 1(1):63–73, January 1970. ISSN 1876-312X, 1399-560X. doi: 10.1163/187631270X00357.
6. Yoshinori Aso and Gerald M Rubin. Dopaminergic neurons write and update memories with cell-type-specific rules. *eLife*, 5:e16135, July 2016. ISSN 2050-084X. doi: 10.7554/eLife.16135.
7. Heather Dionne, Karen L Hibbard, Amanda Cavallaro, Jui-Chun Kao, and Gerald M Rubin. Genetic Reagents for Making Split-GAL4 Lines in Drosophila. *Genetics*, 209(1):31–35, May 2018. ISSN 1943-2631. doi: 10.1534/genetics.118.300682.
8. Haojiang Luan, Nathan C. Peabody, Charles R. Vinson, and Benjamin H. White. Refined spatial manipulation of neuronal function by combinatorial restriction of transgene expression. *Neuron*, 52(3):425–436, November 2006. ISSN 0896-6273. doi: 10.1016/j.neuron.2006.08.028.
9. Barret D Pfeiffer, Teri-T B Ngo, Karen L Hibbard, Christine Murphy, Arnim Jenett, James W Truman, and Gerald M Rubin. Refinement of Tools for Targeted Gene Expression in Drosophila. *Genetics*, 186(2):735–755, October 2010. ISSN 1943-2631. doi: 10.1534/genetics.110.119917.
10. Laszlo Tirian and Barry J. Dickson. The VT GAL4, LexA, and split-GAL4 driver line collections for targeted expression in the Drosophila nervous system. *bioRxiv*, 2017. doi: 10.1101/198648.
11. Lisa Mais, Peter Hirsch, Claire Managan, Kaiyu Wang, Konrad Rokicki, Robert R. Svirskas, Barry J. Dickson, Wyatt Korff, Gerald M. Rubin, Gudrun Ihrke, Geoffrey W. Meissner, and Dagmar Kainmueller. PatchPerPixMatch for Automated 3d Search of Neuronal Morphologies in Light Microscopy. *bioRxiv*, 2021. doi: 10.1101/2021.07.23.453511.
12. Geoffrey W Meissner, Aljoscha Nern, Zachary Dorman, Gina M DePasquale, Kaitlyn Forster, Theresa Gibney, Joanna H Hausenfluck, Yisheng He, Nirmala A Iyer, Jennifer Jeter, Lauren Johnson, Rebecca M Johnston, Kelley Lee, Brian Melton, Brianna Yarbrough, Christopher T Zugates, Jody Clements, Cristian Goina, Hideo Otsuna, Konrad Rokicki, Robert R Svirskas, Yoshinori Aso, Gwyneth M Card, Barry J Dickson, Erica Ehrhardt, Jens Goldammer, Masayoshi Ito, Dagmar Kainmueller, Wyatt Korff, Lisa Mais, Ryo Minegishi, Shigehiro Namiki, Gerald M Rubin, Gabriella R Sterne, Tanya Wolff, Oz Malkesman, and FlyLight Project Team. A searchable image resource of Drosophila GAL4 driver expression patterns with single neuron resolution. *eLife*, 12:e80660, February 2023. ISSN 2050-084X. doi: 10.7554/eLife.80660.
13. Yoshinori Aso, Daisuke Hattori, Yang Yu, Rebecca M Johnston, Nirmala A Iyer, Teri-TB Ngo, Heather Dionne, LF Abbott, Richard Axel, Hiromu Tanimoto, and Gerald M Rubin. The neuronal architecture of the mushroom body provides a logic for associative learning. *eLife*, 3:e04577, December 2014. ISSN 2050-084X. doi: 10.7554/eLife.04577.
14. Arnim Jenett, Gerald M. Rubin, Teri-T. B. Ngo, David Shepherd, Christine Murphy, Heather Dionne, Barret D. Pfeiffer, Amanda Cavallaro, Donald Hall, Jennifer Jeter, Nirmala Iyer, Dona Fetter, Joanna H. Hausenfluck, Hanchuan Peng, Eric T. Trautman, Robert R. Svirskas, Eugene W. Myers, Zbigniew R. Iwinski, Yoshinori Aso, Gina M. DePasquale, Adrianne Enos,

Phuson Hulamm, Shing Chun Benny Lam, Hsing-Hsi Li, Todd R. Laverty, Fuhui Long, Lei Qu, Sean D. Murphy, Konrad Rokicki, Todd Safford, Kshiti Shaw, Julie H. Simpson, Allison Sowell, Susana Tae, Yang Yu, and Christopher T. Zugates. A GAL4-Driver Line Resource for Drosophila Neurobiology. *Cell Reports*, 2(4):991–1001, October 2012. ISSN 2211-1247. doi: 10.1016/j.celrep.2012.09.011.

15. Yoshinori Aso, Daichi Yamada, Daniel Bushey, Karen Hibbard, Megan Sammons, Hideo Otsuna, Yichun Shuai, and Toshihide Hige. Neural circuit mechanisms for transforming learned olfactory valences into wind-oriented movement. *bioRxiv*, 2022. doi: 10.1101/2022.12.21.521497.
16. Nils Otto, Markus W. Pleijzier, Isabel C. Morgan, Amelia J. Edmondson-Stait, Konrad J. Heinz, Ildiko Stark, Georgia Dempsey, Masayoshi Ito, Ishaan Kapoor, Joseph Hsu, Philipp M. Schlegel, Alexander S. Bates, Li Feng, Marta Costa, Kei Ito, Davi D. Bock, Gerald M. Rubin, Gregory S. X. E. Jefferis, and Scott Waddell. Input Connectivity Reveals Additional Heterogeneity of Dopaminergic Reinforcement in Drosophila. *Current Biology*, 30(16):3200–3211.e8, August 2020. ISSN 0960-9822. doi: 10.1016/j.cub.2020.05.077.
17. Sebastian Busch, Mareike Selcho, Kei Ito, and Hiromu Tanimoto. A map of octopaminergic neurons in the Drosophila brain. *The Journal of Comparative Neurology*, 513(6):643–667, April 2009. ISSN 1096-9861. doi: 10.1002/cne.21966.
18. Noa Bielopolski, Hoger Amin, Anthi A Apostolopoulou, Eyal Rozenfeld, Hadas Lerner, Wolf Huetteroth, Andrew C Lin, and Moshe Parnas. Inhibitory muscarinic acetylcholine receptors enhance aversive olfactory learning in adult Drosophila. *eLife*, 8:e48264, June 2019. ISSN 2050-084X. doi: 10.7554/eLife.48264.
19. Julia E. Manoim, Andrew M. Davidson, Shirley Weiss, Toshihide Hige, and Moshe Parnas. Lateral axonal modulation is required for stimulus-specific olfactory conditioning in Drosophila. *Current Biology*, 32(20):4438–4450.e5, October 2022. ISSN 0960-9822. doi: 10.1016/j.cub.2022.09.007.
20. Wendy W. Liu and Rachel I. Wilson. Glutamate is an inhibitory neurotransmitter in the Drosophila olfactory system. *Proceedings of the National Academy of Sciences of the United States of America*, 110(25):10294–10299, June 2013. ISSN 0027-8424. doi: 10.1073/pnas.1220560110.
21. Yoshinori Aso, Robert P Ray, Xi Long, Daniel Bushey, Karol Cichewicz, Teri-TB Ngo, Brandi Sharp, Christina Christoforou, Amy Hu, Andrew L Lemire, Paul Tillberg, Jay Hirsh, Ashok Litwin-Kumar, and Gerald M Rubin. Nitric oxide acts as a cotransmitter in a subset of dopaminergic neurons to diversify memory dynamics. *eLife*, 8:e49257, November 2019. ISSN 2050-084X. doi: 10.7554/eLife.49257.
22. Raphael Cohn, Ianessa Morantte, and Vanessa Ruta. Coordinated and Compartmentalized Neuromodulation Shapes Sensory Processing in Drosophila. *Cell*, 163(7):1742–1755, December 2015. ISSN 1097-4172. doi: 10.1016/j.cell.2015.11.019.
23. Toshiharu Ichinose, Yoshinori Aso, Nobuhiro Yamagata, Ayako Abe, Gerald M Rubin, and Hiromu Tanimoto. Reward signal in a recurrent circuit drives appetitive long-term memory formation. *eLife*, 4:e10719, November 2015. ISSN 2050-084X. doi: 10.7554/eLife.10719.
24. Xiaoliang Zhao, Daniela Lenek, Ugur Dag, Barry J Dickson, and Krystyna Keleman. Persistent activity in a recurrent circuit underlies courtship memory in Drosophila. *eLife*, 7:e31425, January 2018. ISSN 2050-084X. doi: 10.7554/eLife.31425.
25. Brad K Hulse, Hannah Haberkern, Romain Franconville, Daniel Turner-Evans, Shin-ya Takemura, Tanya Wolff, Marcella Noorman, Marisa Dreher, Chuntao Dan, Ruchi Parekh, Ann M Hermundstad, Gerald M Rubin, and Vivek Jayaraman. A connectome of the Drosophila central complex reveals network motifs suitable for flexible navigation and context-dependent action selection. *eLife*, 10:e66039, October 2021. ISSN 2050-084X. doi: 10.7554/eLife.66039.
26. Yoshinori Aso, Divya Sitaraman, Toshiharu Ichinose, Karla R Kaun, Katrin Vogt, Ghislain Belliart-Guérin, Pierre-Yves Plaçais, Alice A Robie, Nobuhiro Yamagata, Christopher Schnaitmann, William J Rowell, Rebecca M Johnston, Teri-T B Ngo, Nan Chen, Wyatt Korff, Michael N Nitabach, Ulrike Heberlein, Thomas Preat, Kristin M Branson, Hiromu Tanimoto, and Gerald M Rubin. Mushroom body output neurons encode valence and guide memory-based action selection in Drosophila. *eLife*, 3:e04580, December 2014. ISSN 2050-084X. doi: 10.7554/eLife.04580.
27. Andrew M. M. Matheson, Aaron J. Lanz, Ashley M. Medina, Al M. Licata, Timothy A. Currier, Mubarak H. Syed, and Katherine I. Nagel. A neural circuit for wind-guided olfactory navigation. *Nature Communications*, 13(1):4613, August 2022. ISSN 2041-1723. doi: 10.1038/s41467-022-32247-7.
28. Daichi Yamada, Daniel Bushey, Feng Li, Karen L Hibbard, Megan Sammons, Jan Funke, Ashok Litwin-Kumar, Toshihide Hige, and Yoshinori Aso. Hierarchical architecture of dopaminergic circuits enables second-order conditioning in Drosophila. *eLife*, 12:e79042, January 2023. ISSN 2050-084X. doi: 10.7554/eLife.79042.
29. Aljoscha Nern, Barret D. Pfeiffer, and Gerald M. Rubin. Optimized tools for multicolor stochastic labeling reveal diverse stereotyped cell arrangements in the fly visual system. *Proceedings of the National Academy of Sciences of the United States of America*, 112 (22):E2967–2976, June 2015. ISSN 1091-6490. doi: 10.1073/pnas.1506763112.
30. Louise E. M. Vet, J. C. Van Lenteren, M. Heymans, and E. Meelis. An airflow olfactometer for measuring olfactory responses of hymenopterous parasitoids and other small insects. *Physiological Entomology*, 8(1):97–106, 1983. ISSN 1365-3032. doi: 10.1111/j.1365-3032.1983.tb00338.x.
31. Tanmay Nath, Guangda Liu, Barbara Weyn, Bassem Hassan, Ariane Ramaekers, Steve De Backer, and Paul Scheunders. Tracking for Quantifying Social Network of Drosophila Melanogaster. In Richard Wilson, Edwin Hancock, Adrian Bors, and William Smith, editors, *Computer Analysis of Images and Patterns*, Lecture Notes in Computer Science, pages 539–545, Berlin, Heidelberg, 2013. Springer. ISBN 978-3-642-40246-3. doi: 10.1007/978-3-642-40246-3_67.
32. Johannes Schindelin, Ignacio Arganda-Carreras, Erwin Frise, Verena Kaynig, Mark Longair, Tobias Pietzsch, Stephan Preibisch, Curtis Rueden, Stephan Saalfeld, Benjamin Schmid, Jean-Yves Tinevez, Daniel James White, Volker Hartenstein, Kevin Eliceiri, Pavel Tomancak, and Albert Cardona. Fiji: an open-source platform for biological-image analysis. *Nature Methods*, 9(7):676–682, July 2012. ISSN 1548-7105. doi: 10.1038/nmeth.2019.
33. Nils Eckstein, Alexander Shakeel Bates, Andrew Champion, Michelle Du, Yijie Yin, Philipp Schlegel, Alicia Kun-Yang Lu, Thomson Rymer, Samantha Finley-May, Tyler Paterson, Ruchi Parekh, Sven Dorkenwald, Arie Matsliah, Szi-Chieh Yu, Claire McKellar, Amy Sterling, Katharina Eichler, Marta Costa, Sebastian Seung, Mala Murthy, Volker Hartenstein, Gregory S. X. E. Jefferis, and Jan Funke. Neurotransmitter Classification from Electron Microscopy Images at Synaptic Sites in Drosophila Melanogaster. *bioRxiv*, 2023. doi: 10.1101/2020.06.12.148775.
34. Expansion-assisted iterative fluorescence in situ hybridization (EASI-FISH) in Drosophila CNS. doi: dx.doi.org/10.17504/protocols.io.5jyl8jmw7g2w/v1.
35. Ann-Shyn Chiang, Chih-Yung Lin, Chao-Chun Chuang, Hsiu-Ming Chang, Chang-Huain Hsieh, Chang-Wei Yeh, Chi-Tin Shih, Jian-Jheng Wu, Guo-Tzau Wang, Yung-Chang Chen, Cheng-Chi Wu, Guan-Yu Chen, Yu-Tai Ching, Ping-Chang Lee, Chih-Yang Lin, Hui-Hao Lin, Chia-Chou Wu, Hao-Wei Hsu, Yun-Ann Huang, Jing-Yi Chen, Hsin-Jung Chiang, Chun-Fang Lu, Ru-Fen Ni, Chao-Yuan Yeh, and Jenn-Kang Hwang. Three-dimensional reconstruction of brain-wide wiring networks in Drosophila at single-cell resolution. *Current biology: CB*, 21(1):1–11, January 2011. ISSN 1879-0445. doi: 10.1016/j.cub.2010.11.056.

Supplemental Videos and Figures.

- Video 1: Comparison of light microscopic images of atypical MBONs with hemibrain skeletons of the corresponding cell types.
- Video 2: Comparison of light microscopic images of typical MBONs with hemibrain skeletons of the corresponding cell types.

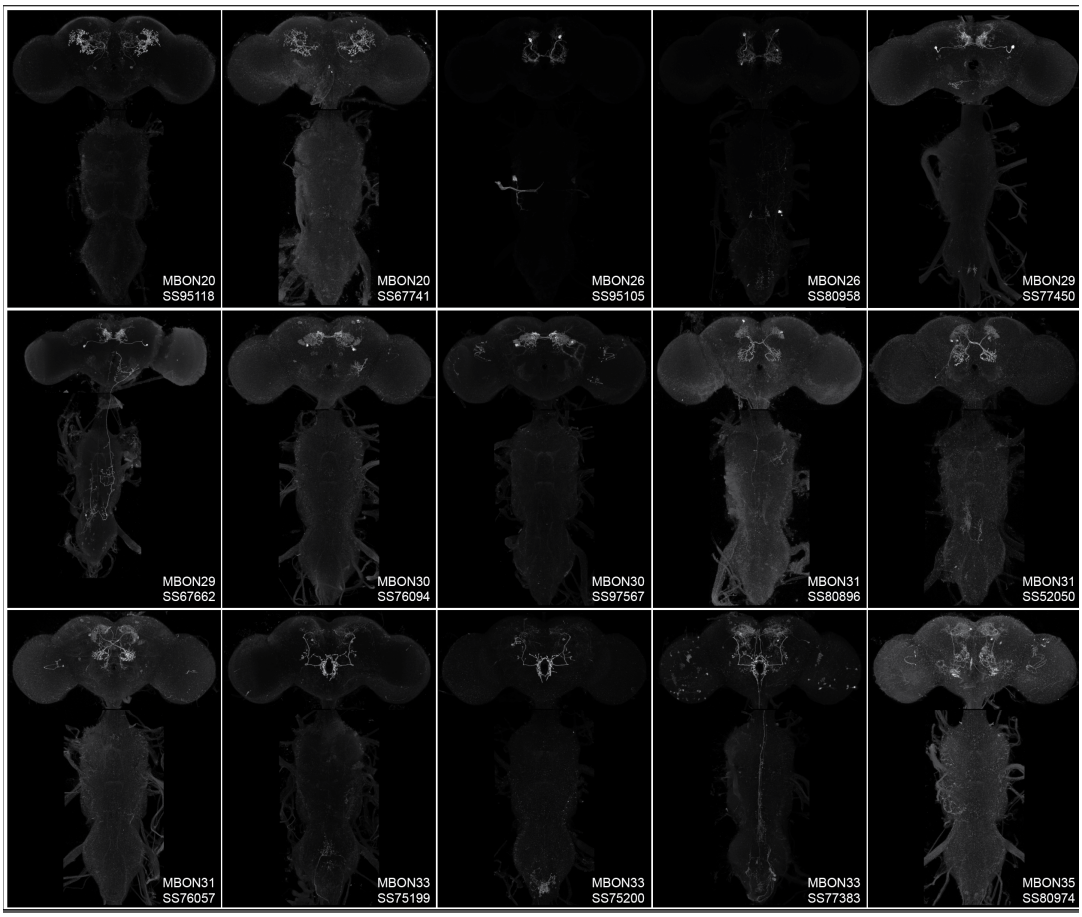

Fig. S1. Maximum intensity projections of the brains and ventral nerve cords of split-GAL4 lines for atypical MBON.

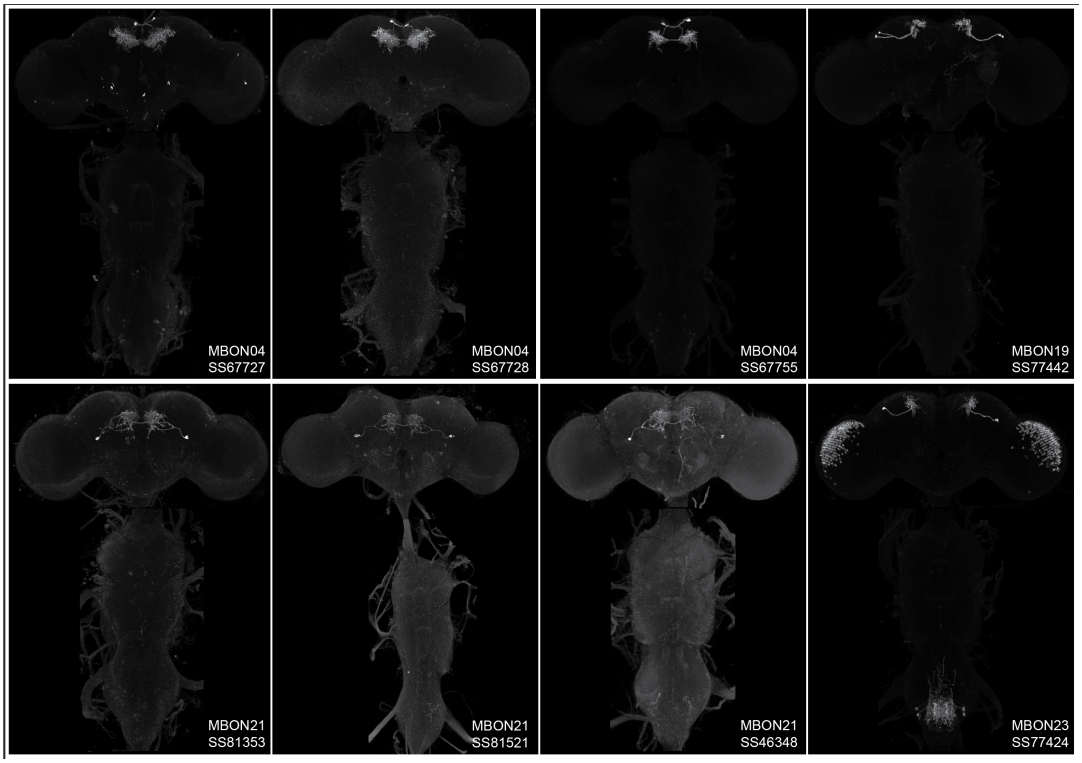

Fig. S2. Maximum intensity projections of the brains and ventral nerve cords of split-GAL4 lines for typical MBON.

	Name	MB Compartments	Transmitter	Number of cells	Drivers
Typical MBONs	MBON01	γ5β′2a	Glutamate	1	**SS01308, MB011B**, **MB210B** (MB002B)
	MBON02	β2β′2a	Glutamate	1	MB399B, **SS01337**
	MBON03	β′2mp	Glutamate	1	**SS01127, MB002B**, **MB011B**, **MB210B**
	MBON04	β′2mp bilateral	Glutamate	1	**SS67727**, **SS67728**, **SS67755** (MB011B)
	MBON05	γ4>γ1γ2	Glutamate	1	**MB434B**, MB298B, SS01188
	MBON06	β1>α	Glutamate	1	**MB434B**, MB433B
	MBON07	α1	Glutamate	2	**MB310C**, **MB323B**, MB319C
	MBON08	γ3	GABA	0 or 1	**MB083C**, **MB110C**
	MBON09	γ3β′1	GABA	1 or 2	**MB083C**, **MB110C**
	MBON11	γ1pedc>α/β	GABA	1	**MB112C**, MB085C, MB262B
	MBON12	γ2α′1	Acetylcholine	2	**MB077B**, MB051B, MB090C
	MBON13	α′2	Acetylcholine	1	**MB018B**, MB091C
	MBON14	α3	Acetylcholine	2	MB082C, MB093C, G0239
	MBON15	α′1	Acetylcholine	4	MB543B, MB618B
	MBON16	α′3ap	Acetylcholine	1	**MB027B**, MB549C, **SS01298**
	MBON17	α′3m	Acetylcholine	2	**MB027B,** MB618B**, SS01298**
	MBON18	α2sc	Acetylcholine	1	**SS01194**, MB549C, MB080C, MB050B
	MBON19	α2p3p	Acetylcholine	2	**SS77442**, MB542B
	MBON21	γ4γ5	Acetylcholine	1	**SS81353, SS81521,**SS46348
	MBON22	calyx	Acetylcholine	1	**SS01388**, MB242A
	MBON23	α2sp	Acetylcholine	1	**SS77424**
Atypical MBONs	MBON10	β′1	GABA	3	MB057B, MB078C
	MBON20	γ1γ2	GABA	1	**SS67741, SS95118**
	MBON24	β2γ5	Acetylcholine	1	none
	MBON25	γ1γ2	Glutamate	1	none
	MBON26	β′2d	Acetylcholine	1	**SS80958, SS95105, SS95109**
	MBON27	γ5d	Acetylcholine	1	none
	MBON28	α′3a	Acetylcholine	1	candidates SS81557, SS86947
	MBON29	γ4γ5	Acetylcholine	1	**SS77450, SS67662**
	MBON30	γ1γ2γ3	Glutamate	1	**SS76094, SS97567**
	MBON31	α′1a	GABA	1	**SS52050,** SS76057**, SS80896**
	MBON32	γ2	GABA	1	none (SS76057 contains MBON31 & MBON32)
	MBON33	γ2γ3	Acetylcholine	1	**SS75199, SS75200**, SS77383
	MBON34	γ2	Glutamate	1	none
	MBON35	γ2	Acetylcholine	1	SS80974

Fig. S3. Summary list of selected split-GAL4 lines for all MBON cell types. These lines represent what we believe to be the best available split-GAL4 drivers for each cell type. The MB compartments they innervate and neurotransmitters are shown. The neurotransmitters that are shaded in gray were assigned based solely on computational prediction (33). Other transmitters have been confirmed by antibody staining (13) or EASI-FISH (34). The number of cells per hemisphere are shown for each cell type. Available split-GAL4 are listed. Lines listed in boldface are generally of higher quality. Lines whose names are shown in purple font were generated as part of this study. Lines whose names are shown in black font were described in (13). Lines from other studies are shown brown font and their sources were as follows: SS01308, (21); G0239, (35); SS46348, (16); MB618B, SS01127, SS01188, SS01194, SS01298, SS01337 and SS01388, Aso 2021 release: https://splitgal4.janelia.org.

A

From		To		
Cell type	transmitter	OANs	Reward DANs	Punishment DANs
MBON01	Glutamate	1	97	49
MBON02	Glutamate	10	116	0
MBON03	Glutamate	0	26	3
MBON04	Glutamate	2	120	11
MBON05	Glutamate	13	333	60
MBON06	Glutamate	4	188	19
MBON07	Glutamate	61	73	0
MBON09	GABA	1	147	48
MBON10	GABA	0	105	124
MBON11	GABA	97	91	96
MBON12	Acetylcholine	0	181	34
MBON13	Acetylcholine	1	78	9
MBON14	Acetylcholine	10	14	30
MBON15	Acetylcholine	2	40	384
MBON16	Acetylcholine	1	0	1
MBON17	Acetylcholine	2	0	4
MBON18	Acetylcholine	4	24	17
MBON19	Acetylcholine	2	1	7
MBON20	GABA	9	6	15
MBON21	Acetylcholine	0	16	141
MBON22	Acetylcholine	2	19	10
MBON23	Acetylcholine	7	169	3
MBON24	Acetylcholine	0	8	15
MBON25	Glutamate	0	35	22
MBON26	Acetylcholine	0	2	4
MBON27	Acetylcholine	1	0	3
MBON28	Acetylcholine	2	0	8
MBON29	Acetylcholine	2	20	131
MBON30	Glutamate	21	140	131
MBON31	GABA	1	209	13
MBON32	GABA	0	0	1
MBON33	Acetylcholine	118	104	5
MBON34	Glutamate	1	6	13
MBON35	Acetylcholine	11	30	106

B

			Punishment DANs		Reward DANs	
			γ1 PPL101	γ3 PAM12	γ4 PAM07, 08	γ5 PAM01
MBON21	γ4γ5	ACh	30	91	12	1
MBON29	γ4γ5	ACh	99	4	9	4
MBON05	γ4	Glu	11	13	285	15
MBON01	γ5β′2a	Glu	0	6	4	47

Fig. S4. Direct connections from MBONs to DANs and OANs. (A) Total number of synaptic connections from each MBON type to DANs and OANs. Based on the valence of memory when activation of DANs is used as unconditioned stimulus in olfactory conditioning (reviewed in (2)) we considered PAM01, 02, 04, 05, 06, 07, 08, 09, 10, 11 and 15 to be Reward DANs and PAM12, 13, 14, PPL101, 103 and 106 to be Punishment DANs. OANs refer to the four types of octopaminergic neurons that innervate the MB: OA-VPM3, OA-VPM4, OA-VUMa2 and OA-VUMa7. (B) Number of connections from MBONs in $\gamma 4$ and $\gamma 5$ to DANs in the γ lobe. PPL103, a DAN in the $\gamma 2$ compartment, has less than five connections with these MBONs and was not included in this table.